Supporting information

Realizing high-performance thermoelectric module through enhancing power factor *via* optimizing carrier mobility in n-type PbSe crystals

Siqi Wang[1], *Yi Wen*[1], *Shulin Bai*[1], *Zhe Zhao*[1], *Yichen Li*[1], *Xiang Gao*[2], *Qian Cao*[3], *Cheng Chang*[1, *], *Li-Dong Zhao*[1, 4*]

[1] *School of Materials Science and Engineering, Beihang University, Beijing 100191, China. E-mail: changchengcc@buaa.edu.cn*; *zhaolidong@buaa.edu.cn*

[2] *Center for High Pressure Science and Technology Advanced Research (HPSTAR), Beijing 100094, China.*

[3] *Huabei Cooling Device Co. LTD., Hebei 065400, China.*

[4] *Tianmushan Laboratory, Yuhang District, Hangzhou 311115, China.*

Supplementary Methods

Synthesis method. All samples were synthesized from high-purity elemental elements, including Pb pieces (99.999%), Se pieces (99.999%), and Al wire (99.999%), and then the chemicals with nominal composition were placed in quartz tubes, sealed at a vacuum of less than 10^{-3} Pa. Crystal is prepared by the temperature gradient method. The raw materials enclosed in pointed quartz tubes were placed into a vertical furnace with a temperature gradient. The temperature was gradually increased from room temperature to 1363 K over 10 h, maintained at this temperature for 3 h, slowly cooled down to 1283 K over 80 h, and finally, the furnace was cooled to room temperature. Crystal samples with a diameter of 13 mm and a length of 40 mm were obtained.

X-ray diffraction (XRD). Diffraction patterns of the powder or cleavage plane for $Pb_{1+x}Se$ (x=0, 0.002, 0.004, 0.006, 0.008) and $Pb_{1.006}Se$+yAl (y = 0, 0.0004, 0.0008, 0.0012, 0.0016, 0.002) crystals were recorded using D/max2200PC instrument with Cu Kα (λ = 1.5418 Å) radiation in a reflection geometry on a diffractometer operating at 20 kV and 20 mA and equipped with a position-sensitive detector.

Electrical transport measurement. The obtained crystals were cut and polished into cuboids with size of ~ 3 × 3 × 10 mm^3. The Seebeck coefficient and conductivity of the samples could be measured simultaneously with Ulvac Riko ZEM-3/CTA instrument in a thin helium atmosphere. It should be noted that the sample surface is coated with a thin layer of boron nitride to prevent contamination of the instrument by possible volatilization. The uncertainty of Seebeck coefficient and conductivity measurements is within 5%.

Thermal transport measurement. The obtained crystals were cut and polished into slices with size of ~ 6 × 6 × 1.5 mm^3 along the same direction as the electrical transport performance measurements. The samples were coated with a thin layer of graphite to reduce the error caused by the emissivity of the material. The total thermal conductivity can be calculated *via* $\kappa=DC_p\rho$, where D is the thermal diffusion coefficient, which could be obtained using Netzsch LFA 457 and analyzed using the Cowan model with pulse correction. C_p represents specific heat capacity, which can be

calculated according to Debye model. ρ represents the density, which can be inferred from the dimensions and mass of the sample. The uncertainty of the total thermal conductivity is within 15% due to errors in measurement or calculation of D, C_p, and ρ.

Hall measurements. The crystal samples to be measured were cut and polished into slices with size of ~6 × 6× 0.6 mm^3. The temperature-dependent hall coefficient R_H was measured using the Van der Paw method on Lake Shore 8400 Series equipment at a reversible magnetic field of 0.9 T with a current of 10 mA. The Hall carrier concentration n_H and the Hall mobility μ_H can be obtained from formulae $n_H = 1/(eR_H)$ and $\mu_H = \sigma R_H$, where e and σ are electron charge and conductivity, respectively.

Microstructure investigation. The PbSe crystals were cut, ground, and polished, then further thinned in Gatan Precision Ion Polishing System (PIPS) II by Ar-ion. The annular dark field scanning transmission electron microscopy (ADF-STEM) images and energy dispersive spectroscopy (EDS) analysis were taken by JEOL JEM-ARM200F scanning transmission electron microscope (STEM) equipped with aberration correction system at an operating voltage of 200 kV.

Defect formation energy calculation. First-principles calculations with projected augmented wave (PAW) pseudopotential formalism were performed within the Perdew-Burke-Ernzerhof (PBE) exchange-correlation functional form of generalized gradient approximation (GGA) method as implemented in the Vienna *Ab-initio* Simulation Package (VASP) software.[1-3] For conduct defect calculations, a 4×4×4 supercell containing 128 atoms for the primitive cell of PbSe structure ($Pb_{64}Se_{64}$) was performed in this work, and the Monkhorst-Pack ***k***-meshes of 3×3×3 was used by the conjugated gradient method to sample in the Brillouin Zone (BZ). The wave functions were adopted in plane wave basis with the kinetic energy cut-off of 550 eV. Due to the presence of heavy Pb element, the spin-orbital coupling effect (SOC)[4] was also separately considered in our calculations, which would affect the bandgaps and the positions of the band edges. The convergence criterions for the total energy and Hellmann-Feynman force were less than 10^{-6} eV and 10^{-2} eV/Å, respectively. The lattice constant and ion position of the perfect supercell were relaxed, while for the

supercells containing defects, the cell volumes were kept constant and the ion positions were relaxed so as to meet the dilute limit condition.[5, 6]

The stability of a defect was determined by its formation energy, which is defined as[6]

$$\Delta H_{\mathrm{d,q}} = E_{\mathrm{d,q}} - E_{\mathrm{pure}} - \sum_i n_i(E_i - \mu_i) + q(E_{\mathrm{V}} + E_{\mathrm{F}} + \Delta V) \quad \text{(S1)}$$

where $\Delta H_{\mathrm{d,q}}$ represents the formation energy of a defect (d) in charge state (q). $E_{\mathrm{d,q}}$ and E_{pure} are the total energy of the defect system and perfect supercell, respectively. n_{i} and E_{i} are the number and total energy of the *i*-th type (host atoms or impurity atoms) added to ($n_i > 0$) or taken from ($n_i < 0$) the supercells in order to create the defect. μ_i refers the corresponding chemical potentials of these atoms, which usually depends on experiment conditions. For a maximally rich growth environment of an element *i*, $\mu_i = 0$. *q* is the corresponding charge value of a charged defect. E_{F} is the Fermi level with respect to E_V, which is the valence band maximum (VBM) of the perfect supercell. ΔV indicates the electrostatic potential difference between the perfect supercell and defective system, which is aligned with the corresponding VBM. The difference of the average electrostatic potential with the atoms far away from the defect sites was adopted in this work.

Fabrication and power generation measurements. The power generation performance of single-leg samples was examined by the Mini-PEM from Advance Riko company, including output power, output voltage, and conversion efficiency. The single-leg samples with dimensions of ~ 3 × 3× 9 mm^3 were created Ni contact layer on the upper and lower surfaces of the samples. To further minimize the contact resistance at the interface, silver pastes were put as a connecting layer between the Cu sheet and the Ni layer. To improve thermal conductivity, silicone grease was applied to the Cu sheet at the high-temperature end. The test temperature difference was 25 K-475 K, and the cold-end temperature was ~298 K.

Fabrication and refrigeration measurements. A 7-pair thermoelectric module

was built to estimate cooling performance using high-performance $Pb_{1.006}Se$+0.0016Al crystal for the *n*-type legs and available Bi_2Te_3 for the *p*-type legs. After adding a Ni layer to the surface of the samples, they were split into 2× 2× 4 mm^3 particles, which were then linked to the copper electrode plates in an interlaced configuration of n-type and p-type particles and welded with Sn-Bi solder. Finally, the 7-pair thermoelectric cooling module with dimensions of 10 mm × 10 mm × 8 mm was prepared, and we used Z-Meters (a commercial thermoelectric cooler test equipment, RMT Ltd., Russia) to allow visual testing of the cooling performance parameters. The cool terminal temperature was maintained at 298 K, while the high-temperature terminals were set at six different temperatures (323 K, 373 K, 423 K, 473 K, 523 K, and 573 K).

***ZT* values calculation.** The average ZT_{ave} value is calculated by:

$$ZT_{ave} = \frac{\int_{T_c}^{T_h} ZT(T)dT}{T_h - T_c}$$

where T_c is the cold-end temperature, and T_h is the hot-end temperature.

Supplementary Figures

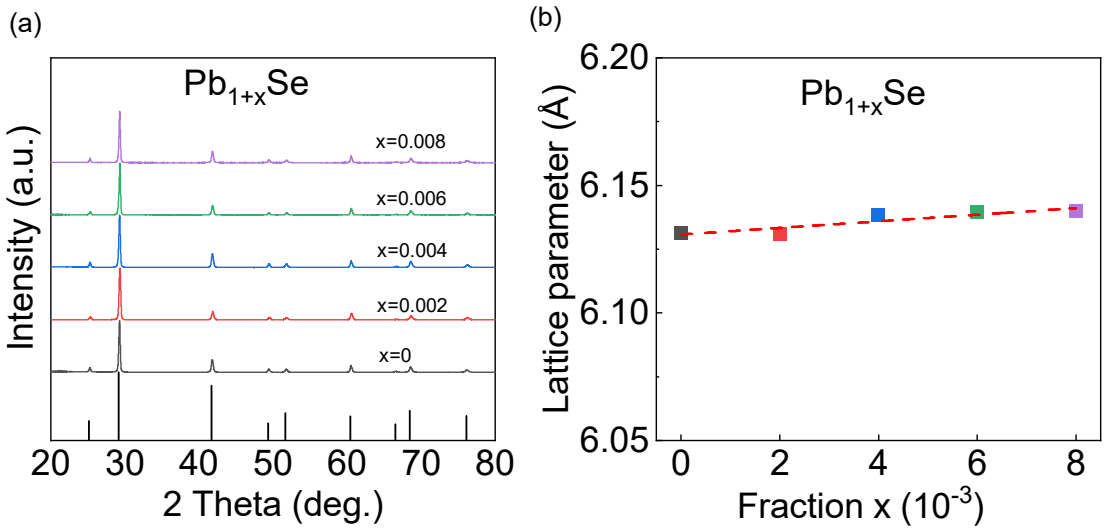

Figure S1. Phase identification of $Pb_{1+x}Se$: (a) Powder XRD pattern; (b) Lattice parameter.

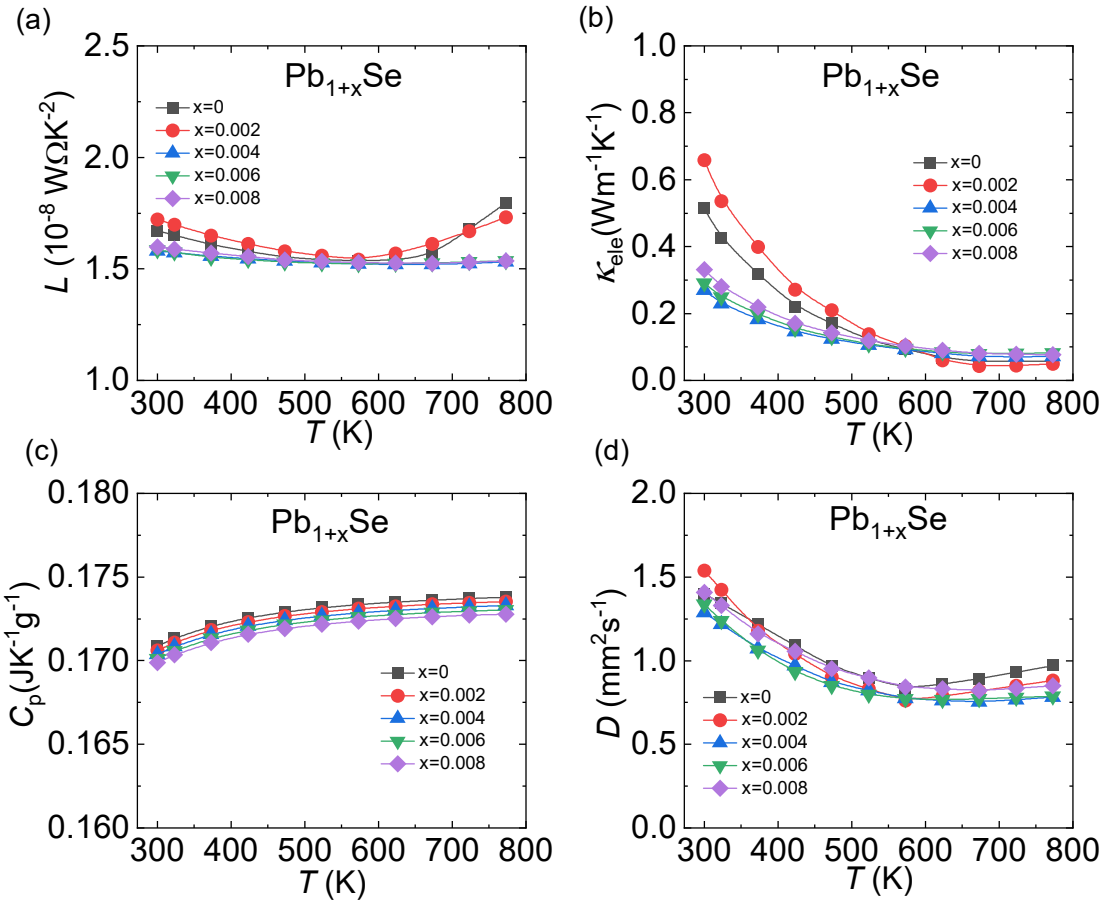

Figure S2. Thermoelectric transport properties of $Pb_{1+x}Se$: (a) Lorenz number; (b) Electronic thermal conductivity; (c) Heat capacity; (d) Thermal diffusivity.

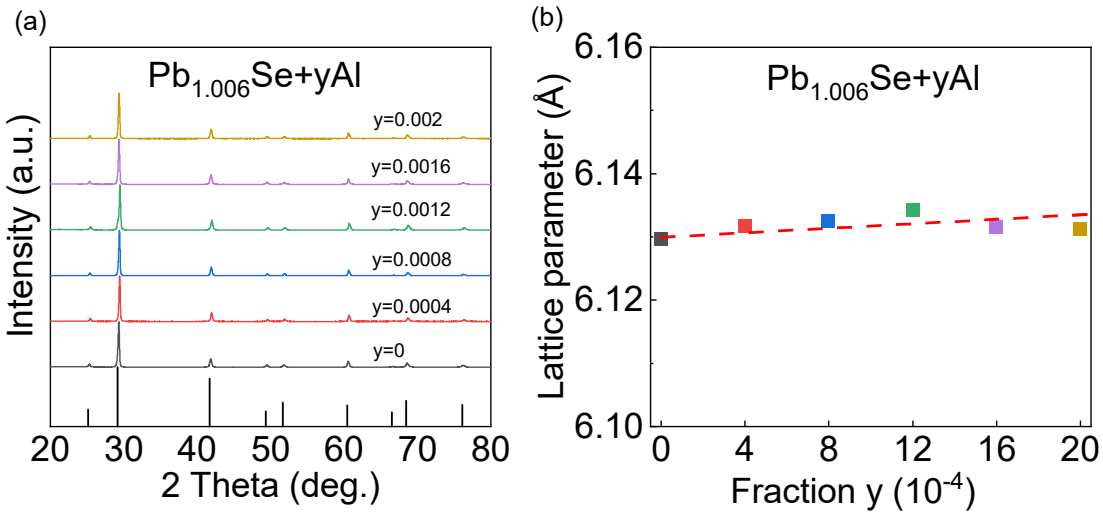

Figure S3. Phase identification of $Pb_{1.006}Se+yAl$: (a) Powder XRD pattern; (b) Lattice parameter.

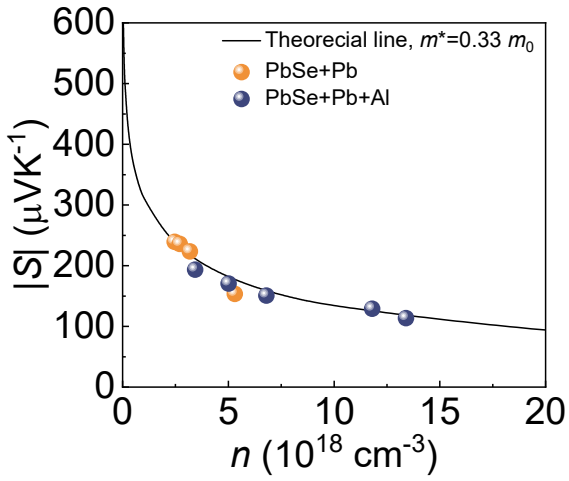

Figure S4. Room-temperature Pisarenko plots.

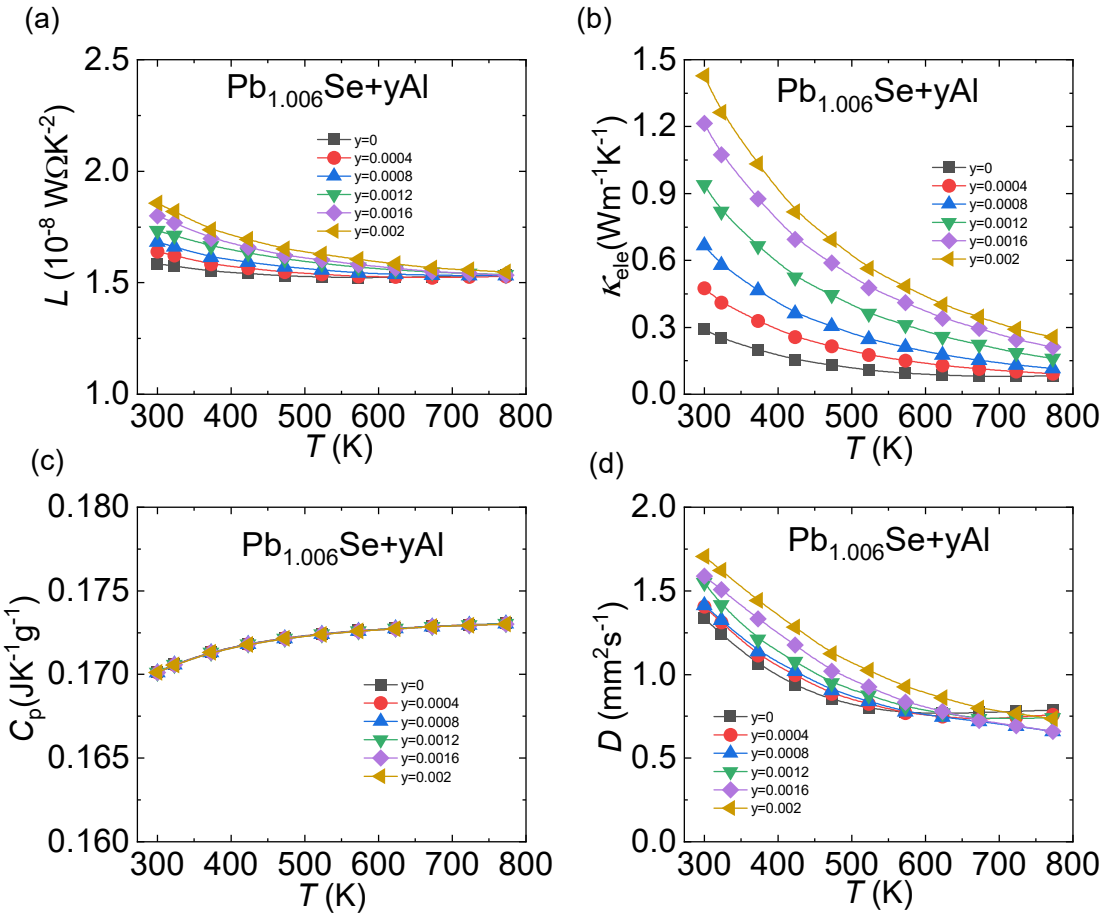

Figure S5. Thermoelectric transport properties of $Pb_{1.006}Se+yAl$: (a) Lorenz number; (b) Electronic thermal conductivity; (c) Heat capacity; (d) Thermal diffusivity.

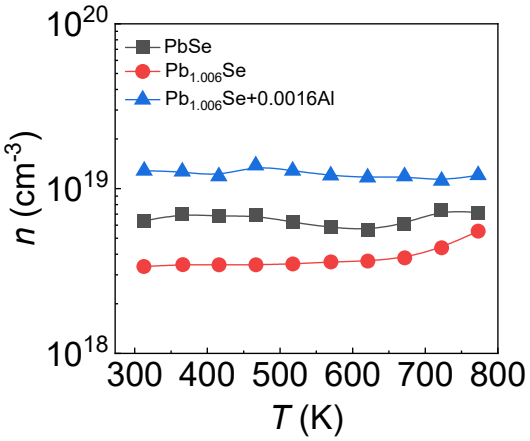

Figure S6. Temperature-dependent carrier concentration.

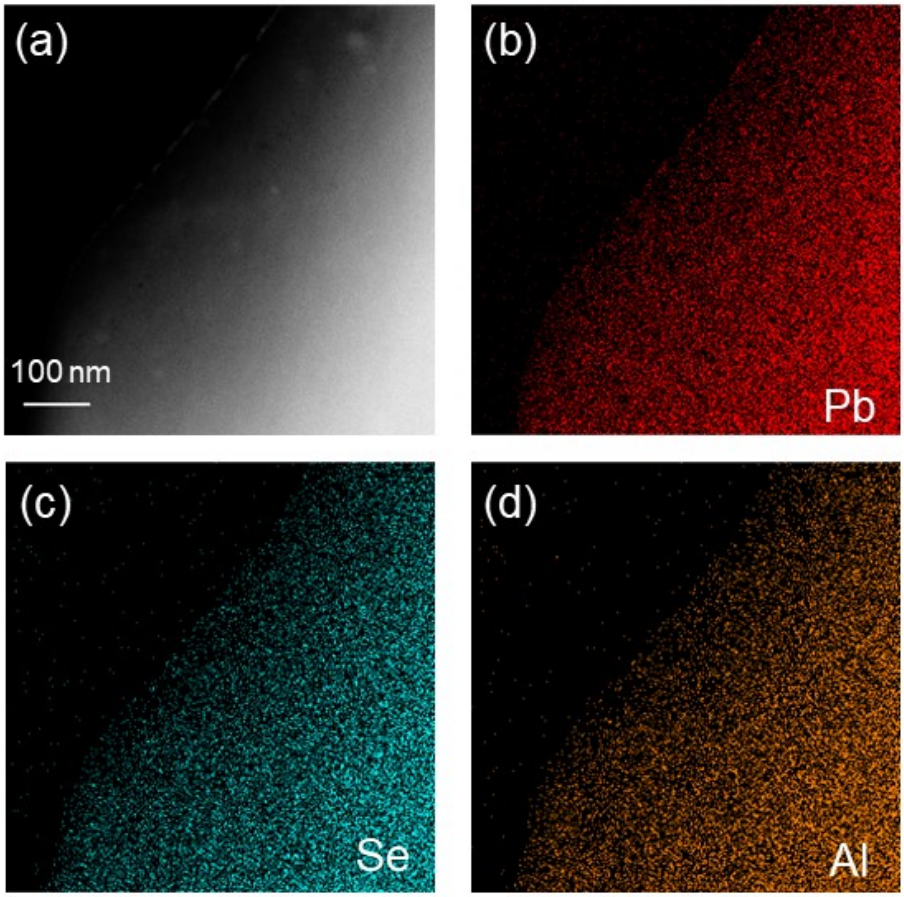

Figure S7. (a) The ADF image and corresponding EDS element maps of (b) Pb, (c) Se, and (d) Al.

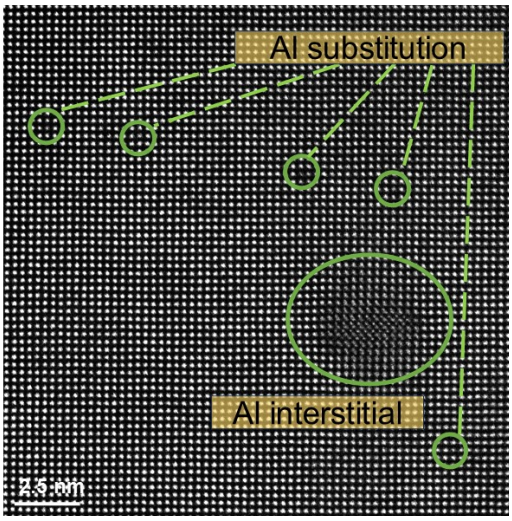

Figure S8. Atom structure observation of PbSe+Pb+Al.

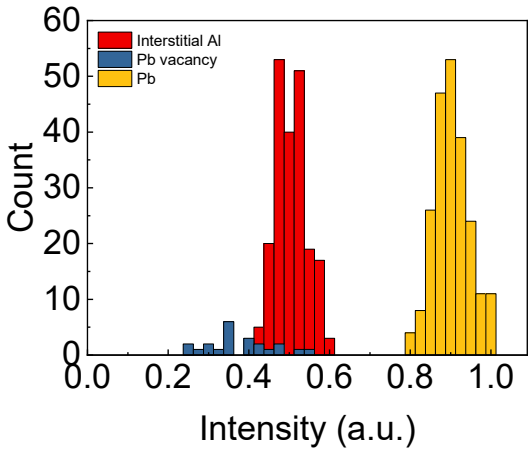

Figure S9. Integrated intensity of each atomic column in Figure 5(f) and Pb vacancies from Figure 5(a) (normalized to the Pb column with highest intensity for comparison).

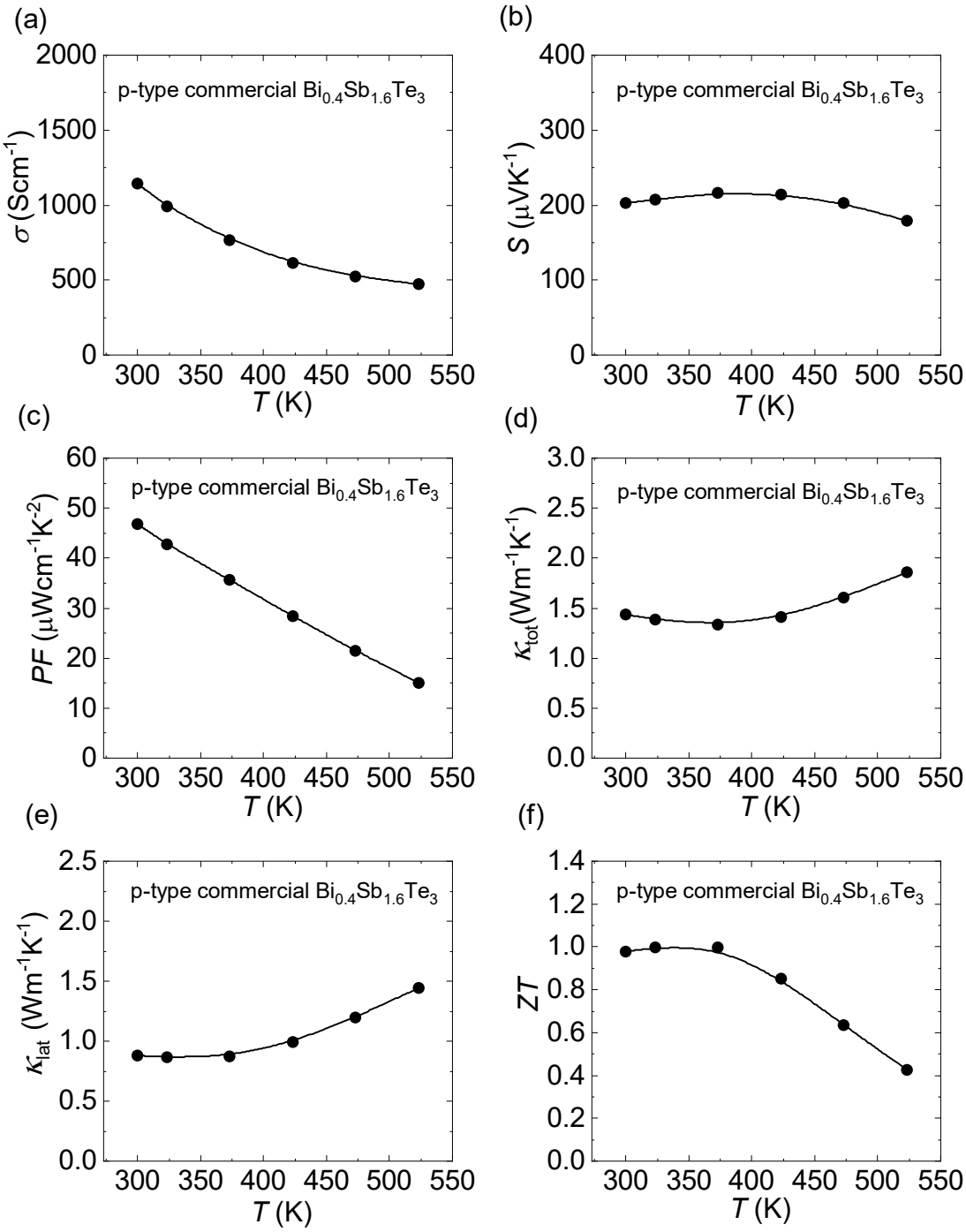

Figure S10. Thermoelectric transport properties of p-type commercial $Bi_{0.4}Sb_{1.6}Te_3$. (a) Electrical conductivity; (b) Seebeck coefficient; (c) Power factor; (d) Total thermal conductivity; (e) Lattice thermal conductivity; (f) *ZT* value.

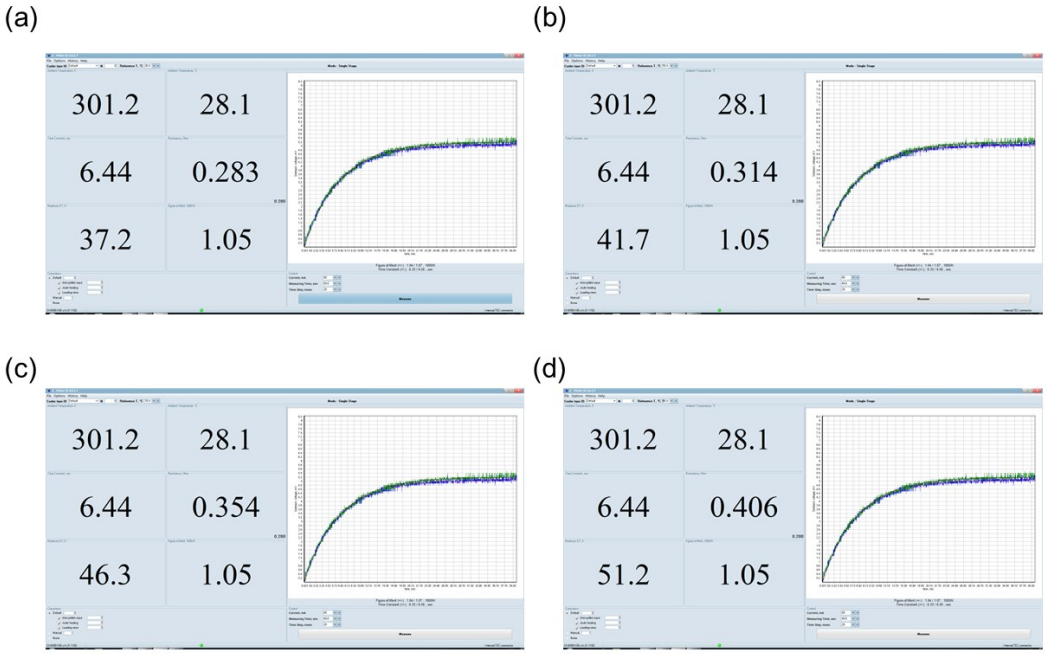

Figure S11. Cooling temperature difference measurement result for a 7-pair thermoelectric module using the Z-Meters equipment (a) at high temperature side T_h ~300 K; (b) at high temperature side T_h ~320 K; (c) at high temperature side T_h ~340 K; (d) at high temperature side T_h ~360 K.

Reference

1. J. Hafner, *J. Comput. Chem.*, 2008, **29**, 2044-2078.
2. K. B. John P. Perdew, Matthias Ernzerhof, *Phys. Rev. Lett.*, 1996, **77**, 3865.
3. P. E. Blochl, *Phys. Rev. B*, 1994, **50**, 17953-17979.
4. M. Filatov and D. Cremer, *J. Chem. Phys.*, 2004, **120**, 11407-11422.
5. J. Vidal, S. Lany, M. d'Avezac, A. Zunger, A. Zakutayev, J. Francis and J. Tate, *Appl. Phys. Lett.*, 2012, **100**, 032104.
6. C. G. Van de Walle and J. Neugebauer, *J. Appl. Phys.*, 2004, **95**, 3851-3879.